PHYSICAL REVIEW E VOLUME 56, NUMBER 3 SEPTEMBER 1997

Pressure statistics for locally isotropic turbulence

Reginald J. Hill[1] and Oluş N. Boratav[2]
[1]*NOAA/ERL/Environmental Technology Laboratory, 325 Broadway, Boulder, Colorado 80303-3328*
[2]*Mechanical and Aerospace Engineering Department, University of California, Irvine, California 92697*
(Received 24 February 1997)

The pressure structure function $D_P(r)$ and pressure-gradient correlation $A_{ij}(\vec{r})$ are related to components of the fourth-order velocity structure function $D_{ijkl}(\vec{r})$ on the basis of the Navier-Stokes equation, incompressibility, local homogeneity, and local isotropy. Data from a wind tunnel, as well as numerical simulation, are used to calculate $D_P(r)$ and thereby show that greater Reynolds numbers are needed to observe an inertial range in $D_P(r)$ than in $D_{ijkl}(\vec{r})$. A previous additional supposition relates $D_P(r)$ and $A_{ij}(\vec{r})$ to the single component $D_{1111}(r)$. This additional supposition is shown to be inaccurate for calculation of $D_P(r)$ and $A_{ij}(\vec{r})$. [S1063-651X(97)50809-9]

PACS number(s): 47.27.Gs

Consider turbulent flow in which kinematic pressure is P and a velocity component is u_i. The pressure structure function is defined by $D_P(r)\equiv\langle(P-P')^2\rangle$, where $\vec{r}=\vec{x}-\vec{x}'$ is the separation vector between two points $\vec{x}$ and $\vec{x}'$ and $r=|\vec{r}|$. Quantities are primed or unprimed if they are evaluated at $\vec{x}$ or $\vec{x}'$, respectively. Angle brackets denote an average. This structure function has been studied theoretically by several investigators [1–8]. The assumption of joint Gaussian velocities or velocity derivatives was used in [2–6]. This joint Gaussian assumption is abbreviated JGA. The pressure structure function, or its spectrum, has also been studied experimentally [6,9,10] and by means of direct numerical simulation (DNS) of the Navier-Stokes equation [11,12]. The pressure structure function is closely related to the pressure-gradient correlation $A_{ij}(\vec{r})$, the mean-squared pressure gradient, and, of course, to the pressure correlation [4,5,7,8]. The pressure-gradient correlation is the dominant term in the correlation of fluid-particle acceleration for high-Reynolds-number turbulence [3–5,13]. Reynolds number is denoted Re and is the root-mean-squared streamwise velocity component multiplied by Taylor's scale and divided by kinematic viscosity.

Under the assumptions of local isotropy, local homogeneity, incompressibility, and by use of the Navier-Stokes equation, $D_P(r)$ is related to the fourth-order velocity structure function [7,8]. The relationship, valid for any Reynolds number, is [7,8]

$$D_P(r)\equiv -\tfrac{1}{3}D_{1111}(r) + \tfrac{4}{3}r^2\int_r^\infty y^{-3}[D_{1111}(y)+D_{\beta\beta\beta\beta}(y)-6D_{11\gamma\gamma}(y)]dy + \tfrac{4}{3}\int_0^r y^{-1}[D_{\beta\beta\beta\beta}(y)-3D_{11\gamma\gamma}(y)]dy, \quad (1)$$

where the fourth-order structure function is $D_{ijkl}(\vec{r})\equiv\langle(u_i-u_i')(u_j-u_j')(u_k-u_k')(u_l-u_l')\rangle$, and where i, j, k, or l is 1 if the velocity component is parallel to the separation vector $\vec{r}$, and 2 or 3 for the orthogonal velocity components perpendicular to $\vec{r}$. Subscripts β or γ each denote either 2 or 3.

Now, Eq. (1) and related equations for pressure-gradient correlation [7,8] could be significantly simplified if relationships exist between the components of $D_{ijkl}(\vec{r})$, similar to the relationships between components of the second-order structure function $D_{ij}(\vec{r})$, and between components of the third-order structure function $D_{ijk}(\vec{r})$. Those latter relationships are based on the fact that the first-order divergence of $D_{ij}(\vec{r})$ vanishes and the second-order divergence of $D_{ijk}(\vec{r})$ vanishes. These divergences vanish on the basis of incompressibility and local homogeneity. An additional simplification based on local isotropy is then used to simplify the relationships. However, no such incompressibility relationship exists between components of $D_{ijkl}(\vec{r})$ because the fourth-order divergence of $D_{ijkl}(\vec{r})$ does not vanish [7,8]; therefore, no order of divergence of $D_{ijkl}(\vec{r})$ vanishes.

On the basis of an analogy with relationships between second- and third-order structure functions, Ould-Rouis *et al.* [14] supposed the relationships

$$D_{11\gamma\gamma}^{\mathrm{OAZA}}(r)=\frac{1}{3}\left(1+\frac{r}{4}\frac{d}{dr}\right)D_{1111}(r) \quad (2a)$$

and

$$D_{\beta\beta\beta\beta}^{\mathrm{OAZA}}(r)=3\left(1+\frac{r}{4}\frac{d}{dr}\right)D_{11\gamma\gamma}^{\mathrm{OAZA}}(r) = \left(1+\frac{r}{4}\frac{d}{dr}\right)\left(1+\frac{r}{4}\frac{d}{dr}\right)D_{1111}(r). \quad (2b)$$

The superscript OAZA is a mnemonic for the authors of [14–16]; the superscript is omitted from $D_{1111}(r)$ because it is obtained from data and thereby generates the other components. If these relationships prove accurate, then they have utility. One use investigated in [15] is the simplification of pressure statistics such as $D_P(r)$. For instance, Eqs. 2(a) and 2(b) substituted in Eq. (1) give [15]

$$D_p^{\mathrm{OAZA}}(r)=\frac{r^2}{3}\int_r^\infty y^{-3}D_{1111}(y)dy-\tfrac{1}{6}D_{1111}(r). \quad (3)$$

Another use of Eqs. 2(a) and 2(b) would be for the calculation of corrections to Taylor's hypothesis because the correction of $D_{ijkl}(\vec{r})$ given in [17] depends on measurements of $D_{1111}(r)$, $D_{\beta\beta\beta\beta}(r)$, and $D_{11\gamma\gamma}(r)$.

Properties of Eqs. 2(a) and 2(b) are as follows. These equations agree in the limit $r\to 0$ with the relationships between fourth-order moments of velocity derivatives that are given in [18]. They agree in the limit $r\to\infty$ with relationships between $D_{1111}(\infty)$, $D_{\beta\beta\beta\beta}(\infty)$, and $D_{11\gamma\gamma}(\infty)$, as given in [7,8]. Those two limit properties at $r\to 0$ and ∞ result from the choice in [14] of values for constants that they introduce. The ratios of components for spacings in the inertial range are [7,8] $H_{\beta\beta}\equiv D_{\beta\beta\beta\beta}(r)/D_{1111}(r)$ and $H_{1\gamma}\equiv D_{11\gamma\gamma}(r)/D_{1111}(r)$. Equations 2(a) and 2(b) give the values $H_{\beta\beta}^{\mathrm{OAZA}}=\frac{16}{9}$ and $H_{1\gamma}^{\mathrm{OAZA}}=\frac{4}{9}$ for the inertial range. These values are in reasonable agreement with measurements [8].

There are reasons to be cautious regarding the accuracy of Eqs. 2(a) and 2(b) for use in Eq. (1). In [7,8], it was found that there is cancellation between terms in Eq. (1). This fact places stringent requirements on the accuracy of Eqs. 2(a) and 2(b). According to [15], isotropy is the only assumption used in [14] to obtain Eqs. 2(a) and 2(b) but careful reading of [14] reveals that isotropy constrains Eqs. 2(a) and 2(b) at only $r=0$ and $r\to\infty$. Proof of the usefulness of Eqs. 2(a) and 2(b) requires experiment or direct numerical simulation. Some aspects of Eqs. 2(a) and 2(b) have been tested in [15,16], but demonstration of the accuracy of Eqs. 2(a) and 2(b) for calculating pressure statistics was inadequate. In Fig. 3 of [16], the comparison of $D_{2222}(r)$ obtained from Eqs. 2(a) and 2(b) with data for $D_{2222}(r)$ shows seemingly significant inaccuracy that [16] attributes to anisotropy, but inaccuracy of Eqs. 2(a) and 2(b) might be the cause. In [7,8], the ratio of the mean-squared pressure gradient $\langle|\partial_i P|^2\rangle$ to the integral $4\int_0^\infty r^{-3}D_{1111}(r)dr$ is denoted by H_χ. In [8], the values $H_\chi=0.36$ and 0.2 were estimated for very small and large Re, respectively. Although it seems that H_χ must vary with Re, Eqs. 2(a) and 2(b) imply the single value $H_\chi^{\mathrm{OAZA}}=0.25$ [15], which suggests that accuracy of Eqs. 2(a) and 2(b) might be limited. The discrepancy between $H_\chi=0.36$ for low Re and $H_\chi^{\mathrm{OAZA}}=0.25$ suggests that, in the dissipation range, $D_P(r)$ is greater than $D_P^{\mathrm{OAZA}}(r)$ by a factor of $0.36/0.25=1.44$ for the case of low Re. Indeed, this discrepancy is observed in Fig. 2 of [15], wherein one sees, at dissipation range spacings, that the normalized values of $D_P(r)$ from DNS at Re=33 are about 40–50 % greater than from use of Eq. (3) with wake data at Re=40.

These cautions led us to compare $D_P(r)$ with $D_P^{\mathrm{OAZA}}(r)$ and compare the corresponding predictions for the pressure-gradient correlation. Nearly isotropic turbulence generated by a grid in a wind tunnel, as well as from direct numerical simulation, was used for this purpose. First, the grid-generated turbulence is described. An X-configuration hot-wire anemometer measured the streamwise velocity component, as well as one cross-stream component. These components are assigned the subscripts 1 and 2, respectively, i.e., $\beta=\gamma=2$. The wires were accurately oriented and calibrated such that $\langle u_2\rangle$ was only 1.5% of $\langle u_1\rangle$. The velocity covariances were $\langle(u_1)^2\rangle=0.135\ \mathrm{m^2\,s^{-2}}$, $\langle(u_2)^2\rangle=0.119\ \mathrm{m^2\,s^{-2}}$, and $\langle u_1u_2\rangle=-0.0036\ \mathrm{m^2\,s^{-2}}$, which show that the turbulence was nearly isotropic. The second- and fourth-order structure-function components $D_{11}(r)$, $D_{22}(r)$, $D_{1111}(r)$, $D_{2222}(r)$, and $D_{1122}(r)$ were calculated from the measured velocities. The numerators of the ratios $D_{12}(r)/D_{11}(r)$, $D_{1112}(r)/D_{1111}(r)$, and $D_{1222}(r)/D_{1111}(r)$ should be zero in isotropic turbulence. These ratios were less than 0.02 for $r<10$ cm. For locally isotropic turbulence, $(r/2)dD_{11}(r)/dr+D_{22}(r)-D_{11}(r)$ should vanish; it is at most $0.015D_{11}(r)$ for $r<6$ cm, further verifying the accuracy of local isotropy for the present data. Kolmogorov's microscale η was 0.31 mm, Taylor's scale was 8.5 mm, the integral scale was 10.8 cm [19], and Re=208. The hot wires were 1.2 mm long. The signals were filtered at 5 kHz. Data were sampled at 10 kHz, and the mean velocity was $10.1\ \mathrm{m\,s^{-1}}$, so the samples were effectively spaced about 1 mm in the streamwise direction. Further experimental details are in [13,19].

Precautions were taken to assure that the data could be used to evaluate the formulas. Because of the spatial averaging by the anemometer and the temporal filtering, reduced credibility must be given to the statistics at $r\leqslant 1$ mm. Correction for inaccuracy of Taylor's hypothesis [17] showed negligible corrections to the calculated pressure statistics as well as to the structure functions [13]. Because of the dissipation-range spectral bump [20–22], the data do not have an inertial range; this bump and the proximity of the energy-containing range give the measured velocity spectrum an apparent power law with an exponent of about $-\frac{5}{3}+0.19$ [13]. Although Re is not large enough for the asymptotic inertial range to fully develop, the apparent power law extends over a factor of 14 in wave number (cf. Fig. 1 of [19]). That is evidence of significant separation of energy-containing and dissipation scales such that inferences can be made about the appearance of or lack of a corresponding power law in $D_P(r)$.

The numerical simulation was a solution of the Navier-Stokes equations in three dimensions using the Fourier pseudospectral method. The resolution was 300^3, which is equivalent to a resolution of 1200^3, considering flow symmetrics. Statistics were calculated from the 300^3 data points at Re=82. Details of the simulation were given in [23]. Variances of all three velocity components are equal. The quantity $(r/2)dD_{11}(r)/dr+D_{22}(r)-D_{11}(r)$ should vanish by local isotropy; it is, at most, $0.028\,D_{11}(r)$ for $r/\eta<70$, and beyond $r/\eta<70$, it increases linearly to $0.16\,D_{11}(r)$ at $r/\eta=100$. Thus, local isotropy is excellent for $r/\eta<70$, but degrades gradually for $r/\eta>70$.

Figure 1 shows $D_P(r)$ from Eq. (1), as well as from the JGA, denoted $D_P^{\mathrm{JG}}(r)$, $D_P^{\mathrm{OAZA}}(r)$ from Eq. (3), the second and third terms in Eq. (1), and the absolute value of the first term in Eq. (1). The formula for $D_P^{\mathrm{JG}}(r)$ is given in [7] and need not be repeated here. Curves in Fig. 1 extend over the range of r for which we have confidence in local isotropy according to the second-order incompressibility test (i.e., $r/\eta<200$ for the wind tunnel data and $r/\eta<80$ for the simulation). For the wind tunnel data, $D_P^{\mathrm{OAZA}}(r)$ from Eq. (3) is consistently about a factor of 3 smaller than $D_P(r)$ from Eq. (1), but both curves have nearly the same slope. A similar observation holds for the simulation, with the exception of the rapid decrease of $D_P^{\mathrm{OAZA}}(r)$ as r/η increases. At most spacings in Fig. 1, $D_P^{\mathrm{OAZA}}(r)$ is closer to $D_P^{\mathrm{JG}}(r)$ than is $D_P(r)$.

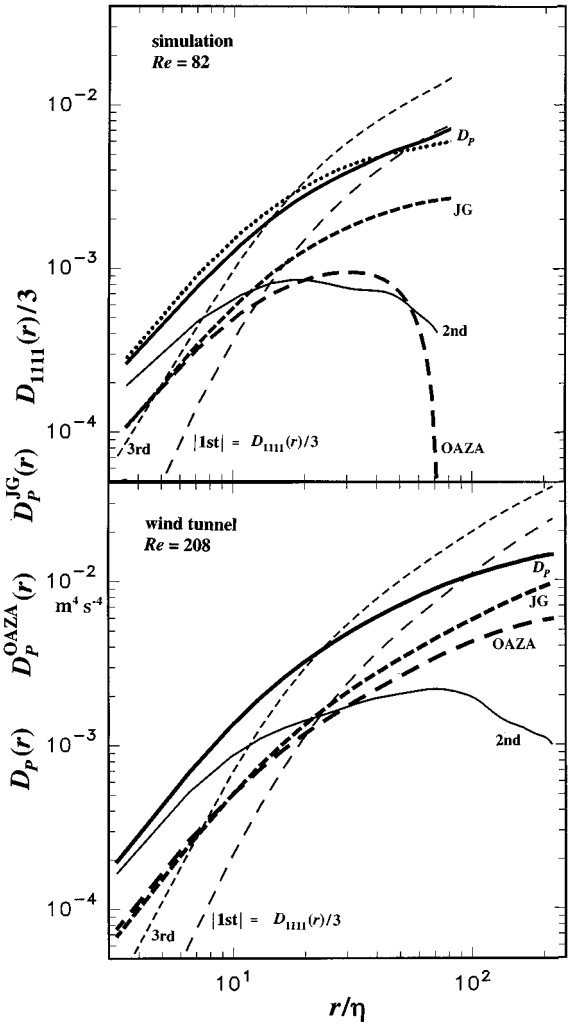

FIG. 1. Upper panel from the simulation; lower panel from the wind tunnel data. Thick curves are the pressure structure function: ———, $D_P(r)$, Eq. (1); – – – –, $D_P^{\mathrm{OAZA}}(r)$, Eq. (3); ----------, $D_P^{\mathrm{JG}}(r)$. Thin curves are the three terms contributing to $D_P(r)$ in Eq. (1): – – – –, first term; ———, second term; ----------, third term. In the upper panel, the dotted curve is $D_P(r)$ directly calculated from the simulation's pressure differences.

Of particular importance is the comparison in Fig. 1 of $D_P(r)$ computed directly from the simulation's pressure differences with $D_P(r)$ from the simulation's $D_{ijkl}(\vec{r})$ substituted in Eq. (1). The difference between these two curves in Fig. 1 is caused by slight local anisotropy in the simulation, and this difference is seen to be very much smaller than the departure of $D_P^{\mathrm{OAZA}}(r)$ from $D_P(r)$. Therefore, the disagreement of $D_P^{\mathrm{OAZA}}(r)$ with data (simulation or wind tunnel) is not caused by any limitation of the computational or measurement methods.

The first term in Eq. (1) cancels by subtraction from the sum of the second and third terms such that $D_P(r)$ is no less than about one-third of the largest magnitude term (the third) anywhere in Fig. 1. Thus, the wind tunnel data are adequate for evaluation of Eq. (1). For $r/\eta > 30$ in Fig. 1, the first term [and therefore $D_{1111}(r)$] has a slope of roughly (4/3) $-2(0.19)$ for the wind tunnel data, which is a somewhat shallower slope than for a fully developed inertial range but

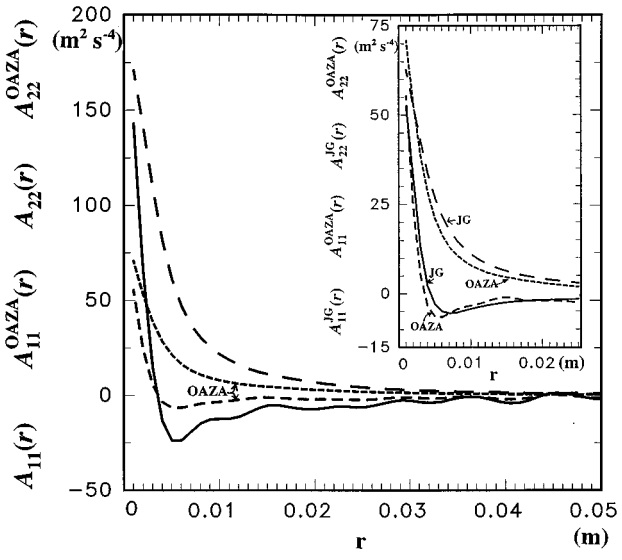

FIG. 2. Pressure-gradient correlation from wind tunnel data: ———, $A_{11}(r)$; – – – –, $A_{11}^{\mathrm{OAZA}}(r)$; — — —, $A_{22}(r)$; ----------, $A_{22}^{\mathrm{OAZA}}(r)$. In the inset of the figure: ———, $A_{11}^{\mathrm{JG}}(r)$; – – – –, $A_{11}^{\mathrm{OAZA}}(r)$; — — —, $A_{22}^{\mathrm{JG}}(r)$; ----------, $A_{22}^{\mathrm{OAZA}}(r)$.

is commensurate with the apparent power law of the wind tunnel velocity spectrum (in Fig. 1 of [19]). For $r/\eta > 30$ in Fig. 1, $D_P(r)$ has a significantly shallower slope (for both the simulation and wind tunnel data) than the first term [i.e., $D_{1111}(r)/3$] because of the cancellation of the first and third terms of Eq. (1) (the second term is negligible for $r/\eta > 30$). Compared with the approach of $D_{1111}(r)$ toward its inertial-range behavior, the shallower slope of $D_P(r)$ indicates that a greater Re is needed for $D_P(r)$ to approach its inertial-range behavior. Independent of intermittency effects, Eq. (1) implies that $D_P(r)$ has inertial-range behavior similar to that of $D_{ijkl}(\vec{r})$ [7,8].

Components of the pressure-gradient correlation, i.e., $A_{ij}(\vec{r}) = \langle (\partial_i P)(\partial_j' P') \rangle$, can be obtained from $D_P(r)$, as follows [5,7,8]:

$$A_{\gamma\gamma}(r) = \frac{1}{2r}\frac{dD_P(r)}{dr}, \quad A_{11}(r) = \frac{1}{2}\frac{d^2 D_P(r)}{dr^2}. \qquad (4)$$

The corresponding formulas in terms of $D_{ijkl}(\vec{r})$ are easily obtained by differentiating Eqs. (1) and (3) and need not be given here. For Eq. (1), the formulas are given in [7,8,13], and for the JGA, the formulas are in [7,13]. Figure 2 shows the comparison of $A_{22}(r)$ and $A_{11}(r)$ obtained from Eqs. (1) and (4) with $A_{22}^{\mathrm{OAZA}}(r)$ and $A_{11}^{\mathrm{OAZA}}(r)$ from Eqs. (3) and (4). Although the DNS data are not shown in Fig. 2, those data corroborate the wind tunnel results, as expected from Eq. (4) and the slopes of the curves in the upper panel of Fig. 1. Consistent with the factor of 3 difference between $D_P(r)$ and $D_P^{\mathrm{OAZA}}(r)$ and the near equality of their slopes for the wind tunnel data in Fig. 1, the two sets of curves in Fig. 2 have nearly the same shape but differ by a factor of about 3. The inset figure of Fig. 2 shows components of $A_{ij}^{\mathrm{OAZA}}(\vec{r})$ from Eqs. (3) and (4) compared with $A_{ij}^{\mathrm{JG}}(\vec{r})$ from the JGA. These components of $A_{ij}^{\mathrm{OAZA}}(\vec{r})$ and $A_{ij}^{\mathrm{JG}}(\vec{r})$ have commensurate

values but somewhat different shapes, as one would expect from the wind tunnel data in Fig. 1 and Eq. (4). That $A_{22}(r)$ is monotonically decreasing with increasing r in Fig. 2 is expected [8,13] on the basis of the monotonic increase of $D_P(r)$. That $A_{11}(r)$ has a minimum where it is negative is required on the basis of local isotropy combined with the fact that the curl of the gradient is zero [13].

In conclusion, an inertial range in $D_P(r)$ will be of more limited extent than in $D_{ijkl}(\vec{r})$ because of the cancellation between terms in Eq. (1). In [14], Eqs. 2(a) and 2(b) are not shown to be exact in any asymptotic case, such as for isotropy or Re$\rightarrow\infty$, except at $r=0$ and $r\rightarrow\infty$ for the isotropic case; therefore, data must be used to check applicability of Eqs. 2(a) and 2(b). Data presented here show that Eqs. 2(a) and 2(b) are not accurate for calculation of $D_P(r)$ or $A_{ij}(\vec{r})$ for the Reynolds number Re=208 or 82. As noted, the data employed have a significant separation of energy-containing scales from dissipation scales and an apparent power law. It therefore seems that applicability of Eqs. 2(a) and 2(b) to calculation of pressure statistics might be of limited accuracy for larger Re than 208. The 40–50 % discrepancy in Fig. 2 of [15] between $D_P(r)$ from numerical simulation and $D_P^{\text{OAZA}}(r)$ from wake data is noted for the case of low Re.

The authors thank S. T. Thoroddsen for use of the data. This work was partially supported by ONR Contract No. N00014-93-F-0038.

[1] W. Heisenberg, Z. Phys. **124**, 628 (1948).
[2] A. M. Obukhov, Dokl. Akad. Nauk SSSR **66**, 17 (1949).
[3] A. M. Yaglom, Dokl. Akad. Nauk SSSR **67**, 795 (1949).
[4] G. K. Batchelor, Proc. Camb. Philos. Soc. **47**, 359 (1951).
[5] A. M. Obukhov and A. M. Yaglom, Prikl. Mat. Mekh. **15**, 3 (1951).
[6] M. S. Uberoi, J. Aeronautical Sci. **20**, 197 (1953).
[7] R. J. Hill, NOAA Technical Report No. ERL 449-ETL **65**, 1993.
[8] R. J. Hill and J. M. Wilczak, J. Fluid Mech. **296**, 247 (1995).
[9] B. G. Jones, R. J. Adrian, C. K. Nithianandan, and H. P. Planchon, AIAA J. **17**, 449 (1979).
[10] W. K. George, P. D. Beuther, and R. E. A. Arndt, J. Fluid Mech. **148**, 155 (1984).
[11] J. C. H. Fung, J. C. R. Hunt, N. A. Malik, and R. J. Perkins, J. Fluid Mech. **236**, 281 (1992).
[12] J. Kim and R. A. Antonia, J. Fluid Mech. **251**, 219 (1993).
[13] R. J. Hill and S. T. Thoroddsen, Phys. Rev. E **55**, 1600 (1997).
[14] M. Ould-Rouis, R. A. Antonia, Y. Zhu, and F. Anselmet, University of Newcastle, Technical Note, No. FM 96/3, 1996 (unpublished).
[15] M. Ould-Rouis, R. A. Antonia, Y. Zhu, and F. Anselmet, Phys. Rev. Lett. **77**, 2222 (1996).
[16] R. A. Antonia, M. Ould-Rouis, Y. Zhu, and F. Anselmet, Europhys. Lett. **37**, 85 (1997).
[17] R. J. Hill, Atmos. Res. **40**, 153 (1996).
[18] N. Phan-Thien and R. A. Antonia, Phys. Fluids **6**, 3818 (1994).
[19] S. T. Thoroddsen, Phys. Fluids **7**, 691 (1995).
[20] S. G. Saddoughi and S. V. Veeravalli, J. Fluid Mech. **268**, 333 (1994).
[21] G. Falkovich, Phys. Fluids **6**, 1411 (1994).
[22] D. Lohse and A. Müller-Groeling, Phys. Rev. Lett. **74**, 1747 (1995).
[23] O. N. Boratav and R. B. Pelz, Phys. Fluids **9** (5), 1400 (1997).